Phys. Status Solidi B **246**, No. 7, 1476–1482 (2009) / **DOI** 10.1002/pssb.200844486

physica status solidi b
www.pss-b.com
basic solid state physics

Magnetization dynamics in polycrystalline Permalloy and epitaxial Co platelets observed by time-resolved photoemission electron microscopy

Frederik Wegelin[1], Alexander Krasyuk[1,2], Dmitrii A. Valdaitsev[1], Sergej A. Nepijko[*,1,3], Hans Joachim Elmers[1], Gerd Schönhense[1], and Claus M. Schneider[4,5]

[1] Institut für Physik, Johannes-Gutenberg-Universität, 55099 Mainz, Germany
[2] Max-Planck-Institut für Mikrostrukturphysik, Weinberg 2, 06120 Halle, Germany
[3] Institute of Physics, National Academy of Sciences of Ukraine, pr. Nauki 46, 03028 Kiev, Ukraine
[4] Institut für Festkörperforschung IFF-6, Forschungszentrum Jülich, 52425 Jülich, Germany
[5] Fachbereich Physik, Universität Duisburg-Essen, 47048 Duisburg, Germany

Received 18 December 2008, revised 4 May 2009, accepted 4 May 2009
Published online 24 June 2009

PACS 31.70.Hg, 75.30.–m, 75.50.Bb, 75.60.Ch, 75.70.Ak, 85.70.Kh, 85.75.–d

[*] Corresponding author: e-mail nepijko@uni-mainz.de, Phone: +49 30 3925412, Fax: +49 30 3923807

We studied the dynamic magnetization response in rectangular polycrystalline Permalloy and also epitaxial Co structures (lateral sizes comprised tens of microns at a thickness of tens of nanometers) during the action of a magnetic field pulse, using time-resolved X-ray photoemission electron microscopy with a time resolution of 10 ps. In the case of Permalloy platelets the restoring torque that is necessary for the stroboscopic image acquisition is provided by the Landau flux closure structure representing a minimum of the free energy. We investigated the dynamic response of 90° Néel domain walls. The main results are: the maximum velocity of the domain wall is 1.5×10^4 m/s, the intrinsic frequency of the magnetization change in these structures is estimated to be several Gigahertz. For the case of epitaxial Co platelets grown on Mo(110) the magnetic uniaxial anisotropy with an easy axis along Mo[$1\bar{1}0$] restores the homogeneous magnetization structure after each field pulse. We observed a rotation of the mean magnetization direction within the first 100 ps of the field pulse.

1 Introduction The dynamic magnetization response is of great importance for the understanding of magnetization reversal processes involving domain patterns and complex magnetic configurations. The knowledge about the microscopic mechanisms determining the time-evolution of these noncollinear magnetization structures is necessary for improving the speed of magnetic data storage devices, for example, of the cells in a magnetic random access memory (MRAM) device [1]. To address this issue, magnetic domains and domain walls must be visualized with a combination of sufficiently high lateral and time resolution. This combination became recently available by methods based on polarized soft X-rays, namely, time-resolved X-ray photoemission electron microscopy (TR-XPEEM) [2–8] and time-resolved X-ray transmission microscopy (TR-XTM) [9, 10]. The XPEEM permits a surface-sensitive approach to magnetodynamic phenomena, whereas XTM yields bulk information. Both employ X-ray magnetic circular dichroism (XMCD) as contrast mechanism.

Characteristic sizes of the magnetic domains range up to the order of several micrometers. Therefore, a high time resolution accompanied by a moderate lateral resolution (several 100 nm) has first been realized in optical techniques, such as magneto-optical microscopy (Kerr/Faraday microscopy) [11] and magneto-optical scanning near-field microscopy (SNOM) [12]. In a time-resolved PEEM, however, the lateral resolution may be better by almost an or-

der of magnitude [13] (down to about 20 nm). In addition, the PEEM approach also enables quantitative measurements of the magnetic stray fields [8, 14] including their dynamics during the magnetic reversal [15, 16] to be carried out. This stray field information complements the results on the magnetodynamics of domains and domain walls. In the present paper, we describe XPEEM studies of the dynamic response of 90° domain walls in Permalloy platelets and of a homogeneous magnetization in epitaxial Co platelets with a time-resolution of about 10 ps, using a special operation mode of the storage ring facility BESSY in Berlin.

2 Experimental details Fast magnetic field pulses were applied via the Oerstedt field of a microstrip line passed by fast current pulses. In the case of Permalloy platelets, the microstrip line of 50 μm width was prepared by means of optical lithography and subsequent wet chemical etching of a 250 nm thick Cu film on a SiO_x/Si substrate. A bilayer (40 nm $Ni_{81}Fe_{19}$, 2 nm Cu) was deposited on top of this microstrip line by DC magnetron sputtering and was microstructured by optical lithography and ion milling. The Cu cap layer served as a protection against oxidation and was removed by mild ion etching after introducing the sample into the photoemission electron microscope. In this paper we concentrate on two rectangular elements of 40 μm × 20 μm and 40 μm × 10 μm in size, i.e. aspect ratio of 2:1 and 4:1, respectively. The single crystalline Mo(110) strip lines were produced in the following way [17]. In the first step, a Mo(110) epitaxial film (200 nm) was deposited on $Al_2O_3(11\bar{2}0)$ in UHV by electron-beam evaporation. During Mo evaporation, the temperature of the substrate was kept constant at 1000 K. In the second step, the strip line (coplanar waveguide with a width of 100 μm of the central lead) and contacts were patterned by standard photolithography. The sample was again transferred into the UHV chamber and in the third step, the Mo strip line was cleaned by repeated cycles of heating in oxygen atmosphere up to 1300 K, followed by flashing at 1800 K in UHV until the Auger electron spectroscopy (AES) signals of C and O originating from the Mo surface were below the detection limit. On this sample a Co layer (20 ML) and a Au capping layer (5 ML) were deposited by molecular beam epitaxy. Epitaxial growth of the Co layer was controlled by low energy electron diffraction (LEED). The Co/Au layer was kept thin enough in order to avoid electrical shorting of the strip line. The final structuring of the platelets on the central lead was performed by focussed ion beam etching (FIB). We also narrowed the central lead on a length of 1 mm to a width of 20 μm in order to increase the Oerstedt field.

The experiment was carried out using the UE52-SGM beamline at the BESSY synchrotron radiation source (Berlin). The magnetic image contrast in the Permalloy particles was obtained via magnetic circular dichroism at the Ni L_3 absorption edge ($h\nu = 853$ eV). For the time-resolved measurements, we used the low-alpha multi-bunch mode

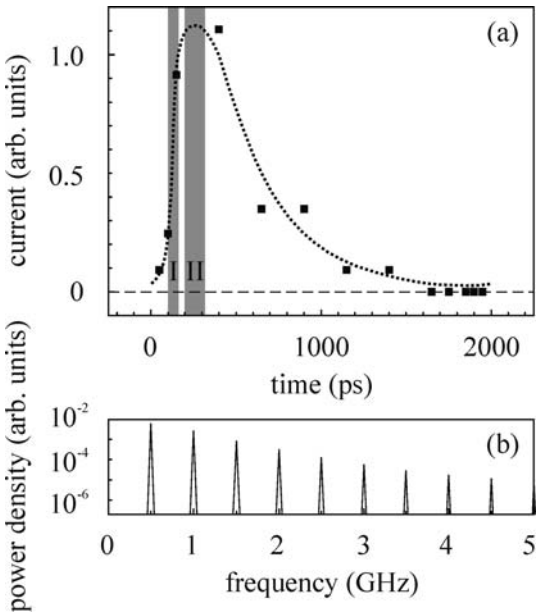

Figure 1 (a) Temporal profile of the magnetic field pulse measured in situ by small image defocusing $\Delta f \neq 0$ (squares represent experimental values). The dashed line denotes a fit with a Fourier series. (b) Corresponding Fourier decomposition of the pulse profile.

of BESSY, which provides photon pulses with a width <2 ps and 2 ns separation (repetition rate 0.5 GHz). The pulse generator used delivered pulse amplitudes of ~7 V with a full width at half maximum (FWHM) of ~100 ps (Fig. 1a) at a frequency of 0.5 GHz phase-locked with the synchrotron frequency. An adjustable delay served to set the time of image acquisition with respect to the magnetic field pulse. The jitter measured by comparing synchrotron trigger and pulse generator output ranged between 8 ps and 14 ps. The rising edge (200 ps) is far shorter than its trailing edge. From previous experiments [5, 18], we know that the pulse shape on the microstrip line area observed in the microscope is narrower than measured outside the UHV system (incl. leads and contacts), thus the rising edge of the field pulse $\sim \boldsymbol{H}(t)$ can be expected to be significantly shorter than 200 ps when it arrives at the magnetic structure. Due to the fast rising edge, frequency components in the 10 GHz range are contained in the Fourier spectrum of the field pulse as shown in Fig. 1b. Further details of the stroboscopic imaging approach performed in the photoemission electron microscope are described in Refs. [5, 16].

The stroboscopic experiment performed here is very much alike to the experiment shown in Fig. 2 in Ref. [18].

The current pulse in Fig. 1a was reconstructed from the deformation of PEEM images of the particles being studied. The deformation was caused by the passage of the current pulse through the microstrip line. This method is described in detail in Refs. [18, 19]. The black squares show the experimental points. A high sensitivity of this method of measuring the pulse profile is realized under

image defocusing $\Delta f \neq 0$. All following measurements of the domain patterns were performed at the condition $\Delta f = 0$. The Fourier spectrum (Fig. 1b) was determined by fitting the pulse profile (Fig. 1a) by a Fourier series $A(t) = \sum_n A_n \sin n\omega t$, A_n denotes the amplitudes of the Fourier components n. Obviously, the steep rising edge contains significant Fourier frequencies up to several Gigahertz.

3 Experimental results and their discussion The effect of the magnetic field pulses on the micropatterns is shown in Fig. 2a–h, which compiles a sequence of images taken with a time increment of $\Delta t = 10$ ps. The light incidence (projection onto the sample surface) and the pulse field $\sim \boldsymbol{H}(t)$ are directed from left to right (parallel to the short edge of the particles) and bottom-up (parallel to the long edge of the particles), respectively, as given in the inset. Due to the alignment between the local magnetization and the direction of light incidence, only three distinct contrast levels (black, white and gray) appear. The XMCD-PEEM image in Fig. 2a shows the domain structures of the particles under study at $t = 100$ ps, i.e. at the onset of the field pulse. These structures are schematically shown by solid lines and are very similar to the initial flux closure (Landau) domain patterns of the structures involved. Following the evolution of this pattern in time, we observe that the domain structure is visibly affected, i.e., the magnetization distribution is locally deformed. The domain boundaries shift significantly within the next 10 ps ($t = 110$ ps), see Fig. 2b. The dotted lines in Fig. 2b mark the new position of the domain boundaries, as given by the contrast changes from black to white. These field-induced changes may be emphasized, if the domain pattern from Fig. 2a is subtracted from the image in Fig. 2b (see Fig. 2c). Figure 2c–h shows a series of difference images calculated from image pairs taken at subsequent points in time $t = 110$ (c), 120 (d), 130 (e), 140 (f), 150 (g), 160 ps (h) and $t^* = t - \Delta t$ ($\Delta t = 10$ ps). The fact that these difference XPEEM images exhibit distinct features indicates two important findings. First, the actual time resolution is significantly smaller than the chosen step width. Second, the observed changes are reversible and appear during all (or at least most) of the cycles in our stroboscopic experiment. The results of measurements given in Fig. 2a–h correspond to the current pulse leading-edge (100 ps $\leq t \leq$ 160 ps), denoted as area I in Fig. 1a.

A closer inspection of the data in Fig. 2 reveals that the changes during the time sequence are mostly confined to the domain boundaries. They change more in the larger left particle than in the smaller right one. In addition, the changes do not follow a simple trend, but rather an almost oscillatory pattern, although we are still on the rising edge of the pulse. This shows up very clearly when comparing Fig. 2c and e, in which the contrast indicating the response of the domain boundaries is reversed. Therefore, the behavior of the magnetization at the domain boundaries is more complex and cannot be described by a simple linear motion, i.e. a domain wall shift as in the case discussed in Ref. [6]. It further proves the significance of the higher Fourier frequencies contained in the steep rising edge (see Fig. 1b).

In the further course of the field pulse changes occur at different locations in the magnetization pattern, as depicted in the sequence in Fig. 3a–g. In the following, we will concentrate on the dynamic behavior in the region close to the maximum of the field pulse (Fig. 1a, area II). Near the flat maximum the overall response is weaker than during the rising edge which again points on the importance of the Fourier components with a strong damping of these high-frequency modes in the particle. In this sequence the

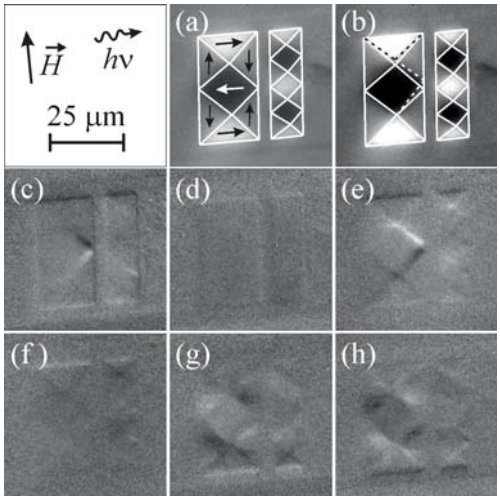

Figure 2 XMCD-PEEM images of Permalloy particles taken during the steep rising edge of the field pulse at $t = 100$ (a) and 110 ps (b) as well as difference images calculated from image pairs taken at $t = 110$ (c), 120 (d), 130 (e), 140 (f), 150 (g) and 160 ps (h) and $t^* = t - \Delta t$, $\Delta t = 10$ ps. Directions of light incidence (projection on the sample surface) and pulse field $\boldsymbol{H}$ are indicated in the inset.

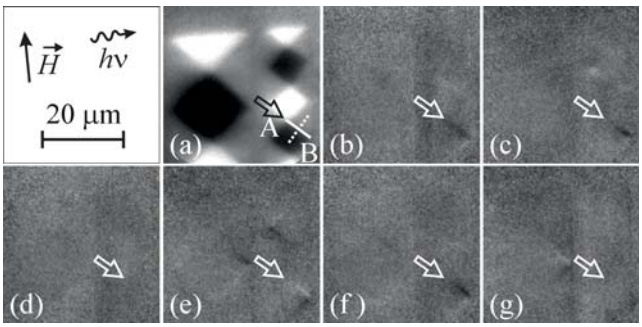

Figure 3 XMCD-PEEM images of Permalloy particles taken in the region of the pulse maximum at $t = 200$ ps (a) and difference images corresponding to the pairs $t = 220$ (b), 240 (c), 260 (d), 280 (e), 300 (f) and 320 ps (g) and $t^* = t - \Delta t$, $\Delta t = 20$ ps. Line AB denotes the 90° Néel domain wall. Near the line AB the contrast of the region marked by a thick arrow with white border varies (b–g).

smaller particle shows a contrast whereas the larger one yields practically no response. Figure 3b–g demonstrates the changes in the magnetization distribution in the area containing the 90° Néel wall marked by the line AB (see Fig. 3c) between the domains in the Landau pattern. The difference XMCD-PEEM images taken at the points in time $t = 220$ (b), 240 (c), 260 (d), 280 (e), 300 (f), 320 ps (g) and $t^* = t - \Delta t$ ($\Delta t = 20$ ps), map the evolution in time. As can be seen, close to the line AB the contrast in the region marked by the white arrow varies distinctly. This is caused by a change of the magnetization direction in the region adjoining the 90° Néel domain wall AB. The dynamics of this contrast change is compiled in Fig. 4a. It gives a series of intensity profiles $j(x)$ through the region under study extracted from the XMCD-PEEM images taken between $t = 200$ ps and 300 ps. These profiles are recorded along the dotted line being perpendicular to the line AB (Fig. 3a). Since the grey level in the XMCD contrast is proportional to $\cos\alpha$, where α is the angle between the directions of magnetization in the particle plane and projection of direction of illumination onto this plane. The angular dependence $\alpha(x)$ (Fig. 4a, right hand scale) can be directly extracted from the intensity profiles $j(x)$ (Fig. 4a, left hand scale). The extremal values $\alpha = 180$ and 270° on the right-hand scale correspond to the grey levels for the magnetization direction being antiparallel and perpendicular to the projected photon impact direction, respectively. We clearly see that the profiles $\alpha(x)$ in Fig. 4a shift to the right and deform as t increases. This is a further indication that we cannot interpret the series of curves in Fig. 4a in terms of a quasi-static movement of the 90° Néel domain wall AB.

The vertical dashed line in Fig. 4a corresponds to the centre of the region marked by the white arrow in Fig. 3b–g. From the variation of $\alpha(x)$ along this line, we can extract the time dependence of the angle $\alpha(t)$ as shown in Fig. 4b. An inaccuracy in the determination of the angles can be caused by the fact that not all of the 10^{13} cycles of the passage of the magnetic field pulse are characterized by complete repeatability, or there is a non-negligible out-of-plane component of the transient magnetization. It means that the real curve $\alpha(t)$ can be shifted to somewhat higher angles. As is seen in Fig. 4a, the monotonous character of the shift of the intensity profile lines $j(x)$ is disturbed from the left to the right with increasing t. This can be induced by the above-mentioned effect as well as by the wave character of spin wave propagation. The latter reason is the most probable and it can explain an oscillating variation of the position and inversion of the contrast of the region marked by the arrow in Fig. 3b–g.

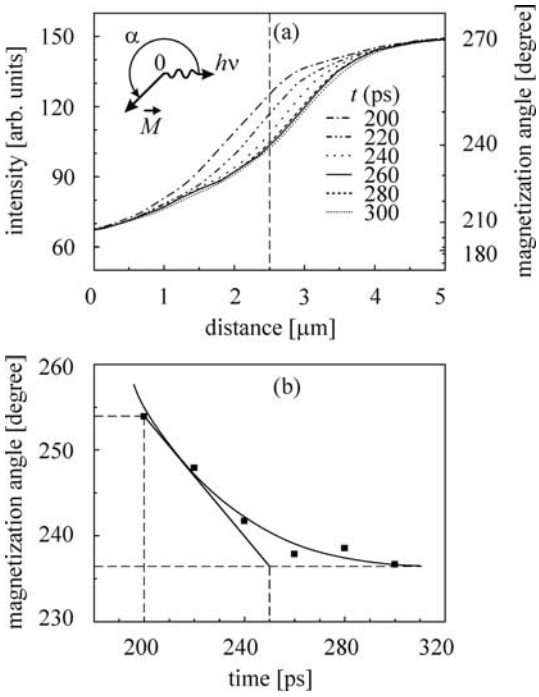

Figure 4 (a) Intensity profiles $j(x)$ along the dotted line designated in Fig. 3a for the XMCD asymmetry images taken at the times $t = 200$, 220, 240, 260, 280 and 300 ps. The right ordinate gives the angle dependence $\alpha(x)$. The magnetization angle α is counted from the illumination direction (its projection on the particle plane) as depicted in the inset. The dashed line denotes the centre of the region marked by the arrow with white border in Fig. 3b–g and corresponds to the position of line AB in Fig. 3a. (b) The local magnetization direction $\alpha(t)$ in the region marked by the arrow in Fig. 3b–g as function of time.

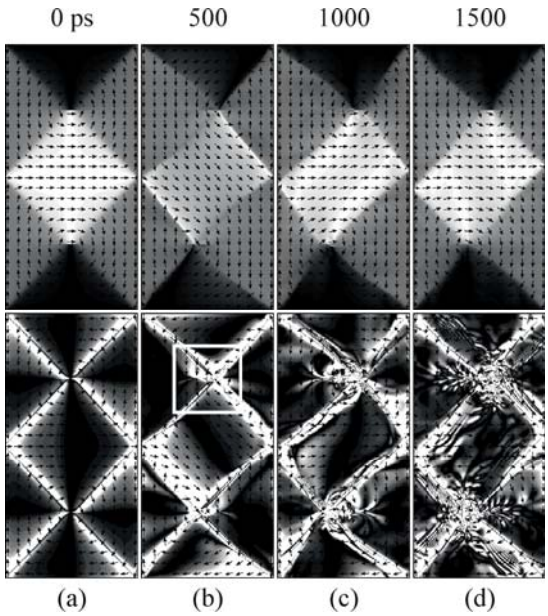

Figure 5 Emission of spin waves from 90° Néel domain walls (simulation using the NIST OOMMF code [20]). Top panel: Micromagnetic simulation results showing the time evolution of the magnetization (bright areas are magnetized to the right, dark areas to the left) in a Permalloy particle with linearly reduced dimensions (4 μm × 2 μm × 10 nm) for delay times $t = 0$ (a), 500 (b), 1000 (c) and 1500 ps (d). Bottom panel: Corresponding divergence of the magnetization on the surface of the particle.

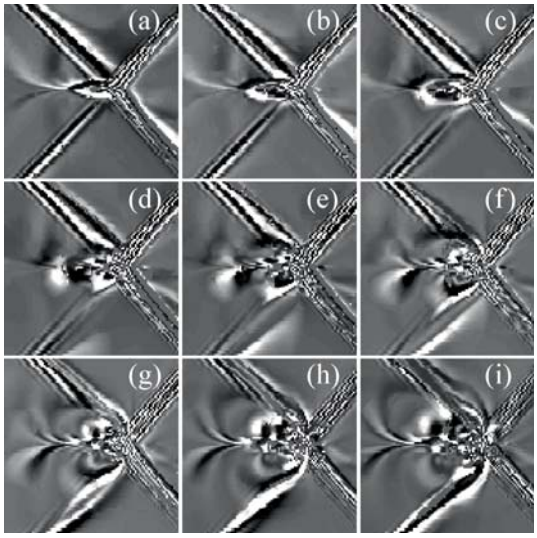

Figure 6 Difference images of magnetization divergence for the area designated by the white square in Fig. 5 at the times t = 550 (a), 600 (b), 650 (c), 700 (d), 750 (e), 800 (f), 850 (g), 900 (h) and 950 ps (i) and $t^* = t - \Delta t$, Δt = 50 ps.

Any change of the magnetic configuration on such a short time scale is accompanied by the emission of spin waves. The top panel of Fig. 5 shows the result of a simulation of spin waves generated at a 90° Néel domain wall. This computer simulation was realized with the help of the program described in Ref. [20] for a Permalloy particle of rectangular shape with aspect ratio 2:1. The magnetic field pulse profile was chosen similar to the measured one shown in Fig. 1a. The local directions of magnetization are denoted with small arrows. The calculations were carried out with a step width of 10 ps. The results of simulation of spin waves, which are distant from each other 500 ps, are given in the top panel of Fig. 5. From the comparison of adjacent images, one sees distinct shifts of 90° Néel domain walls and corresponding deformations of the domains themselves. They agree in the essential features with the experimentally observed shifts. The stronger local magnetic fields are, the larger are the shifts. The magnetic divergence is visualized in the bottom panel of Fig. 5 with a step width of 500 ps. In more detail, these variations with steps of 50 ps for the area designated by the white square in Fig. 5 are illustrated by the difference images of the divergence in Fig. 6.

Considering the high Fourier frequency components in our experiments, we can assume that particular spin wave modes are driven almost into a resonant behavior, comparable, for example, to a parametric oscillator. It has also been shown recently that spin waves may propagate through domain walls [21]. The overlap of these spin wave modes and the noncollinear magnetization distribution in the domain wall itself gives rise to a local variation of the magnetization and may explain the deformation of the profiles observed in Fig. 4a. We can try to estimate the period of this mode from Fig. 4b. It can be determined from the condition that the magnetization direction in the spin wave should change by $\alpha = 360°$ during a full period. The period T is equal to few hundred picoseconds (the frequency is few Gigahertz) because, as is seen from Fig. 4b, the turn of the magnetization direction reaches 4° in 10 ps. The characteristic time of the magnetic reversal ($\alpha = 180°$) is $T/2$. A movement of a 90° Néel domain wall means that in the region of the domains adjacent to the wall, on one side the magnetization direction turns by the angle of $\alpha = 90°$ and becomes parallel to the domain magnetization direction on its other side. It means that the second domain grows on the expense of the first domain, and in such a manner the domain wall moves. The characteristic time needed for this process comprises $T/4$, i.e. a few hundreds of picoseconds. This result generally confirms the data available in the literature [11]. For example, the study of the magnetization dynamics of similar samples performed by means of Kerr effect (square Permalloy particles with edge lengths of order of a few microns and 18 nm thick) showed that the intrinsic frequency of the magnetization reversal comprised modes of a few Gigahertz [11]. Besides, the frequency is characterized by the dimensional dependence (it increases as the particle lateral size decreases). Similar results supporting the experimental findings were obtained from Landau–Lifshitz–Gilbert simulations [11].

The velocity of the 90° Néel wall AB is determined from the shift along the abscissa of the profiles in Fig. 4a taken with time increments of Δt = 20 ps. The maximum velocity is 1.5×10^4 m/s.

Figure 7 shows the time dependence of the field pulse generated by the epitaxial strip line on Al_2O_3. Due to the small damping in the Al_2O_3 substrate compared to the Si substrate used for the Permalloy platelets the field pulse shows an equally sharp leading and trailing edge, reproducing exactly the output of the pulse generator. The maximum field amplitude calculated from the current signal measured after the pulse has passed the strip line amounts to 6 mT. Co films grown on Mo(110) show a uniaxial anisotropy with the easy axis along the Mo[1 $\bar{1}$0] direction, that in turn is aligned with the strip line axis [17]. The anisotropy constant determined from Kerr magnetometry measured before the final FIB structuring is $K_p = 0.47 \times 10^5$ J/m^3 corresponding to a saturation field of $\mu_0 H$ = 50 mT. The deviation from the results measured for Mo capped Co/Mo(110) films [17] might be attributed to the surface anisotropy induced by the Au capping. Moreover, a decrease of the magnetic anisotropy due to structural damage in the course of the FIB structuring has to be taken into account.

The uniaxial anisotropy defines the magnetization direction at equilibrium along the strip line. A homogeneous magnetization state as shown in Fig. 7a is typical for an epitaxial film. The dark colour of the platelet in Fig. 7a indicates a magnetization component antiparallel to the incident X-ray beam before the field pulse arrives. During the start of the field pulse we observe a reversal of the XMCD asymmetry revealing a change of sign of the horizontal

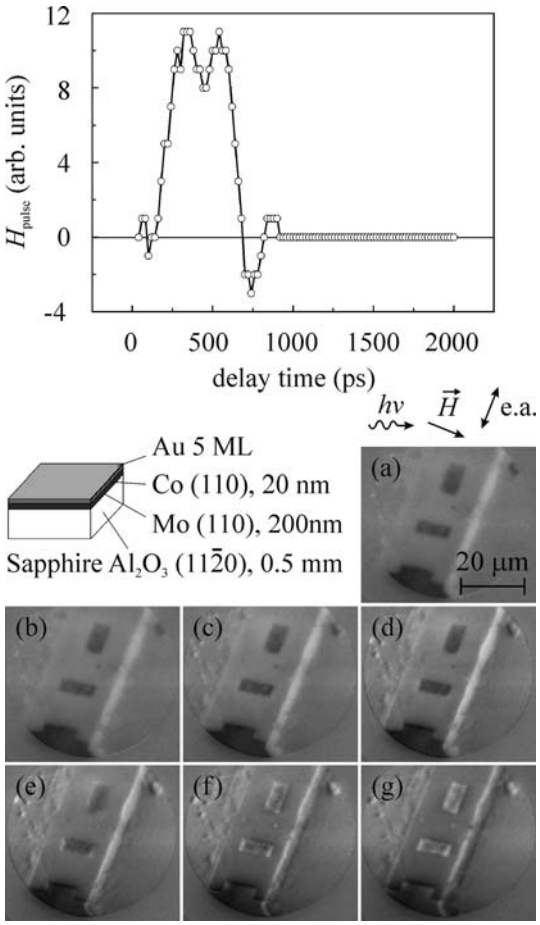

Figure 7 Time-resolved XMCD-PEEM of epitaxial Co platelets on a single-crystalline Mo(110) strip line on $Al_2O_3(11\bar{2}0)$. Top: Temporal profile of the magnetic field pulse $H_{pulse}(t)$. Bottom: Sequence (a–g) showing the change of magnetization state with time steps of Δt = 20 ps. The series was taken in the rising edge of the field pulse. Sizes of Co particles on the strip line are 5 µm × 10 µm and 10 µm × 5 µm.

magnetization component. Consequently, the magnetization has rotated by at least 45° in Fig. 7g. A quasi-static field of 6 mT would only cause a small rotation of 7° for the given field and anisotropy. This unexpected large response might be attributed to a decreased magnetic anisotropy deviating from the measurement on the unstructured area of the sample.

In addition, we observe a non-uniform response of the magnetization. Close inspection of Fig. 7f–g reveals a larger positive asymmetry (positive horizontal magnetization component) at the short edges of the rectangle that is oriented with its long axis along the field and at the long edges of the rectangle that is oriented with its short axis along the field. This observation indicates a stronger dynamic response of the magnetization at the edges where the field enters and leaves the magnet. This is quite surprising since one would expect a stronger response just at the other edges because of the demagnetizing field occurring at the poles of the magnetic sample. On the other hand the demagnetizing field is negligibly small for the ultrathin film investigated here and a lateral inhomogeneous magnetic anisotropy due to the structuring might be the reason for his observation.

4 Conclusions We applied a stroboscopic pump–probe technique for the investigation of the dynamics of ferromagnetic particles response to a transient pulse of the magnetic field (resulting from a current pulse through a microstrip line). The time resolution is determined by the photon pulse width as well as the jitter of the bunch-marker and current pulse generator output. In the performed measurements in the low-alpha multi-bunch mode of BESSY the photon pulse width was <2 ps and the jitter was about 10 ps. The resulting total time resolution was thus essentially restricted by the jitter. It is determined by the pulse electronics, the length of the connecting cables etc. and can be decreased down to a few picoseconds. It means that a time resolution of a few picoseconds can be achieved with the help of the applied technique.

The high time resolution allowed us to study the dynamics of the deformation of 90° Néel walls in Permalloy structures with a Landau flux closure pattern due to the action of a magnetic field pulse on these particles. The characteristic time for magnetization reversal estimated from this comprises $T/2$ (the period T is equal to few hundreds of picoseconds and the intrinsic precession frequency $f = T^{-1}$ amounts to a few Gigahertz). We observed a fast response within 100 ps of the magnetization within an epitaxial Co platelet grown on an epitaxial Mo(110) strip line.

Acknowledgements This work was supported by the DFG (priority program "magnetization dynamics") and BMBF (project 03N6500). Thanks are due to the BESSY staff and, in particular, H. Schmitz and W. Braun for excellent support and I. Mönch and J. Vinzelberg for sample preparation.

References

[1] J. Åkerman, Science **308**, 508 (2005).
[2] J. G. Schönhense, A. Oelsner, A. Krasyuk, C. M. Schneider, M. Bauer, and M. Aeschlimann, in: Recent Trends in Charged Particle Optics (Czechoslovak Microscopy Society, Brno, 2002, ISBN 80-238-8986-9), pp. 87–90.
[3] S.-B. Choe, Y. Acremann, A. Scholl, A. Bauer, A. Doran, J. Stöhr, and H. A. Padmore, Science **304**, 420 (2003).
[4] J. Vogel, W. Kuch, M. Bonfim, J. Camarero, Y. Pennec, F. Offi, K. Fukumoto, J. Kirschner, A. Fontaine, and S. Pizzini, Appl. Phys. Lett. **82**, 2299 (2003).
[5] A. Krasyuk, A. Oelsner, S. A. Nepijko, A. Kuksov, C. M. Schneider, and G. Schönhense, Appl. Phys. A **76**, 863 (2003).
[6] A. Krasyuk, F. Wegelin, S. A. Nepijko, H. J. Elmers, G. Schönhense, M. Bolte, and C. M. Schneider, Phys. Rev. Lett. **95**, 207201 (2005).
[7] J. Raabe, C. Quitmann, C. H. Back, F. Nolting, S. Johnson, and C. Buehler, Phys. Rev. Lett. **94**, 217204 (2005).

[8] C. M. Schneider, A. Kuksov, A. Krasyuk, A. Oelsner, D. Neeb, S. A. Nepijko, G. Schönhense, J. Morais, C. de Nadai, and N. B. Brookes, Appl. Phys. Lett. **85**, 2562 (2004).
[9] H. Stoll, A. Puzic, B. van Waeyenberge, P. Fischer, J. Raabe, M. Buess, T. Haug, R. Höllinger, C. Back, D. Weiss, and G. Denbeaux, Appl. Phys. Lett. **84**, 3328 (2004).
[10] B. van Waeyenberge, A. Puzic, H. Stoll, K. W. Chou, T. Tyliszczak, R. Hertel, M. Fähnle, H. Brückl, K. Rott, G. Reiss, I. Neudecker, D. Weiss, C. H. Back, and G. Schütz, Nature **444**, 461 (2006).
[11] J. P. Park, P. Eames, D. M. Engebretson, J. Berezovsky, and P. A. Crowell, Phys. Rev. B **67**, 020403 (2003).
[12] J. Levy, V. Nikitin, J. M. Kikkawa, A. Cohen, N. Samarth, R. Garcia, and D. D. Awschalom, Phys. Rev. Lett. **76**, 1948 (1996).
[13] S. A. Nepijko, A. Oelsner, A. Krasyuk, A. Gloskovskii, N. N. Sedov, C. M. Schneider, and G. Schönhense, Appl. Phys. A **78**, 47 (2004).
[14] S. A. Nepijko, M. Klais, A. Oelsner, G. H. Fecher, G. Schönhense, U. Muschiol, C. M. Schneider, S. Zennaro, N. Zema, and N. N. Sedov, Appl. Phys. A **74**, 259 (2002).
[15] A. Krasyuk, A. Oelsner, S. A. Nepijko, N. N. Sedov, A. Kuksov, C. M. Schneider, and G. Schönhense, Appl. Phys. A **79**, 1925 (2004).
[16] G. Schönhense, H. J. Elmers, S. A. Nepijko, and C. M. Schneider, Time-Resolved Photoemission Electron Microscopy, in: Advances in Imaging and Electron Physics, Vol. 142, edited by P. W. Hawkes (Academic Press, Amsterdam, London, San Diego, 2004), pp. 159–326.
[17] D. A. Valdaitsev, A. Kukunin, J. Prokop, H. J. Elmers, and G. Schönhense, Appl. Phys. A **80**, 731–734 (2005).
[18] D. Neeb, A. Krasyuk, A. Oelsner, S. A. Nepijko, H. J. Elmers, A. Kuksov, C. M. Schneider, and G. Schönhense, J. Phys.: Condens. Matter **17**, S1381 (2005).
[19] C. M. Schneider, A. Kuksov, A. Krasyuk, A. Oelsner, S. A. Nepijko, and G. Schönhense, J. Electron Spectrosc. Relat. Phenom. **144**–**147**, 967 (2005).
[20] http://math.nist.gov/oommf/.
[21] R. Hertel, W. Wulfhekel, and J. Kirschner, Phys. Rev. Lett. **93**, 257202 (2004).

